Accepted Manuscript

Synthesis and evaluation of frentizole-based indolyl thiourea analogues as MAO/ABAD inhibitors for Alzheimer's disease treatment

Lukas Hroch, Patrick Guest, Ondrej Benek, Ondrej Soukup, Jana Janockova, Rafael Dolezal, Kamil Kuca, Laura Aitken, Terry K. Smith, Frank Gunn-Moore, Dominykas Zala, Rona R. Ramsay, Kamil Musilek

PII: S0968-0896(16)31452-3
DOI: http://dx.doi.org/10.1016/j.bmc.2016.12.029
Reference: BMC 13456

To appear in: *Bioorganic & Medicinal Chemistry*

Received Date: 30 November 2016
Accepted Date: 18 December 2016

Please cite this article as: Hroch, L., Guest, P., Benek, O., Soukup, O., Janockova, J., Dolezal, R., Kuca, K., Aitken, L., Smith, T.K., Gunn-Moore, F., Zala, D., Ramsay, R.R., Musilek, K., Synthesis and evaluation of frentizole-based indolyl thiourea analogues as MAO/ABAD inhibitors for Alzheimer's disease treatment, *Bioorganic & Medicinal Chemistry* (2016), doi: http://dx.doi.org/10.1016/j.bmc.2016.12.029

Synthesis and evaluation of frentizole-based indolyl thiourea analogues as MAO/ABAD inhibitors for Alzheimer's disease treatment

Lukas Hroch[a,b], Patrick Guest[c], Ondrej Benek[b,d], Ondrej Soukup[b], Jana Janockova[b], Rafael Dolezal[b,d,e], Kamil Kuca[b,d], Laura Aitken[c], Terry K. Smith[c], Frank Gunn-Moore[c], Dominykas Zala[c], Rona R. Ramsay[c*], Kamil Musilek[b,d*]

[a] *Charles University in Prague, Faculty of Pharmacy in Hradec Kralove, Department of Pharmaceutical Chemistry and Drug Control, Heyrovskeho 1203, 500 05 Hradec Kralove, Czech Republic*

[b] *University Hospital, Biomedical Research Center, Sokolska 581, 500 05 Hradec Kralove, Czech Republic.*

[c] *University of St. Andrews, School of Biology, Medical and Biological Sciences Building or Biomedical Sciences Research Complex, North Haugh, St. Andrews KY16 9ST, United Kingdom*

[d] *University of Hradec Kralove, Faculty of Science, Department of Chemistry, Rokitanskeho 62, 500 03 Hradec Kralove, Czech Republic; kamil.musilek@gmail.com*

[e] *University of Hradec Kralove, Faculty of Informatics and Management, Center for Basic and Applied Research, Rokitanskeho 62, 500 03 Hradec Kralove, Czech Republic*

Abstract

Alzheimer's disease (AD) is a neurodegenerative disorder associated with an excessive accumulation of amyloid-beta peptide (Aβ). Based on the multifactorial nature of AD, preparation of multi-target-directed ligands presents a viable option to address more pathological events at one time. A novel class of asymmetrical disubstituted indolyl thioureas have been designed and synthesized to interact with monoamine oxidase (MAO) and/or amyloid-binding alcohol dehydrogenase (ABAD). The design combines the features of known MAO inhibitors scaffolds (e.g. rasagiline or ladostigil) and a frentizole moiety with potential to interact with ABAD. Evaluation against MAO identified several compounds that inhibited in the low to moderate micromolar range. The most promising compound (**19**) inhibited human MAO-A and MAO-B with IC_{50} values of 6.34 μM and 0.30 μM, respectively. ABAD activity evaluation did not show any highly potent compound, but the compound series allowed identification of structural features to assist the future development of ABAD inhibitors. Finally, several of the compounds were found to be potent inhibitors of horseradish peroxidase (HRP), preventing the use of the Amplex™ Red assay to detect hydrogen peroxide produced by MAO, highlighting the need for serious precautions when using an enzyme-coupled assay.

Keywords

Alzheimer's disease (AD); monoamine oxidase (MAO); amyloid-beta peptide (Aβ); mitochondrial amyloid-binding alcohol dehydrogenase (ABAD); 17β-hydroxysteroid dehydrogenase type 10 (17β-HSD10); horseradish peroxidase (HRP).

1. Introduction

Alzheimer's disease (AD) is the most common cause of senile dementia and is characterized by a progressive impairment of cognitive functions including memory, language and motor skills.[1,2] Though the aetiology of AD still remains unclear, there are several established factors contributing to the progress of AD including e.g. alteration in neurotransmitter systems, deposition of amyloid beta peptide (Aβ), tau-protein hyperphoshorylation with tangle formation, oxidative stress and mitochondrial dysfunction.[3,4]

Most of the currently marketed drugs (namely donepezil, rivastigmine, galanthamine) prevent the degradation of acetylcholine via the inhibition of acetylcholinesterase to sustain sufficient levels in the face of the decreased numbers of cholinergic neurons in AD.[5] This approach is only effective for symptomatic treatment of mild and moderate cognitive decline and does not provide prevention of disease progression.[6] Alongside the well-established dysregulation of cholinergic system, the impairment of other neurotransmitter systems (e.g. dopaminergic or serotonergic) is also present in the brain of AD patients, causing behavioural syndromes in AD patients.[7] Thus, monoamine oxidases (MAO), enzymes responsible for the metabolism of monoamine neurotransmitters, were suggested as possible targets for AD treatment.[8] MAO occurs in two isoforms (MAO-A and MAO-B) with different substrate and inhibitor specificities.[8–10] Alterations of both MAO-A and MAO-B activities (elevated enzyme levels or changes in expression in various brain regions) were reported in AD patient brains.[11–13] While elevated levels of MAO-B are well-described, changes in MAO-A activity are rather more complex and unclear.[14] In the periphery, inhibition of MAO-A can contribute to potential side effects, in particular to tyramine-induced hypertension (also referred as the "cheese effect"). It is induced by dietary amines after the irreversible inhibition of intestinal MAO-A where the inhibitor is covalently bound to the enzyme (via hydrazine or propargyl-amino moiety).[8] Furthermore, elevated levels of the MAO isoforms can also generate toxic metabolites (e.g. aldehydes or hydrogen peroxide),[15] which consequently promote already ongoing oxidative stress in AD.[16] Taken together, targeting both MAO-A and MAO-B could potentially contribute to therapeutic effects in AD treatment.

Besides the neurotransmission anomalies, one of the most widely accepted AD hypothesis focuses on the pathological production of Aβ leading to formation of insoluble extracellular Aβ plaques.[17,18] Intra-mitochondrial Aβ deposition has been associated with mitochondrial dysfunction and impaired synaptic trafficking resulting in neuronal damage.[19,20] Thus, Aβ interactions with mitochondrial proteins may become

therapeutic targets for cellular protection in AD.[21] Several mitochondrial proteins have been shown to interact directly with Aβ, possibly influencing mitochondrial metabolism.[22] The amyloid-binding alcohol dehydrogenase (ABAD) enzyme, also known as 17β-hydroxysteroid dehydrogenase type 10 (17β-HSD10), is one such Aβ binding protein.[23] The Aβ-ABAD interaction promotes the enzyme to undergo functional changes, resulting in altered enzymatic activity, elevated levels of toxic metabolites, enhanced oxidative stress and mitochondrial and synaptic dysfunction.[24–26] Studies using an ABAD decoy peptide consisting of the ABAD amino acid residues responsible for interaction with Aβ, have been shown to disrupt the interaction between ABAD and Aβ, reducing Aβ-induced mitochondrial and neuronal toxicity and improving learning and memory in AD mice models.[25,27] Further, the direct inhibition of the ABAD enzyme has been shown to have neuroprotective effects in terms of reducing cell stress via decreased generation of reactive oxygen species, improved mitochondrial respiration, and stabilization of estradiol levels.[28,29] Thus both the direct inhibition of ABAD enzyme and the disruption of the Aβ-ABAD interaction present possible approaches for AD treatment.[29]

Due to the multifactorial nature of AD aetiology, the question whether a single-target-directed drug could yield therapeutic effect in AD treatment has led scientists to focus still more on the emerging multi-target-directed ligand (MTDL) approach.[30] Simultaneous modulation of several pathological events of the ongoing disease may then contribute to therapeutic effect of progressing AD.[31] The MTDL approach has been employed by many research groups[32–35] and has shown success, for example in the case of the compound ladostigil[36] which has reached clinical trials.[37] Exploiting the advantage of conjunctive approach, we designed a series of compounds combining known scaffolds of MAO and ABAD inhibitors to introduce MAO inhibitory activity into frentizole moiety and explore structural inhibitory features of both MAO and ABAD scaffolds. Xie *et al*. observed that the FDA approved drug, frentizole (Fig. **1**: **A**), acted as a weak inhibitor of the Aβ-ABAD interaction (IC_{50} = 200 μM) and described a novel class of frentizole-based benzothiazolyl (thio)ureas acting as inhibitors of the Aβ-ABAD interaction.[38] Relatively minimal modifications of the distal phenyl ring substitution also allowed phosphonate analogues of the same scaffold to act as direct ABAD inhibitors, yielding two compounds that inhibited ABAD with IC_{50} values of 52.7 μM and 341.9 μM.[39,40] Recently, low micromolar scale ABAD inhibitors were reported.[41] Furthermore, a fused bicyclic system comprised of 5- and 6-membered rings (i.e. indane) represents core scaffold of several MAO inhibitors (e.g. rasagiline or ladostigil). The carbocyclic system is not exclusive for MAO inhibition, since other bicyclic and heterocyclic scaffolds have been reported to inhibit MAO.[35,42] In this case, the aminoindane moiety has been replaced with an isosteric indole ring (Fig. **1**: **B**) and further incorporated into frentizole scaffold (Fig. **1**: **A**). The frentizole urea linker was changed to the analogous thiourea linker since the similar thiocarbonyl scaffold was previously identified to be beneficial for ABAD inhibition.[43] The distal phenyl ring presented in frentizole was modified by various substitution patterns that have been introduced to investigate structure and activity relationship of this scaffold (Fig. **1**: **C**).

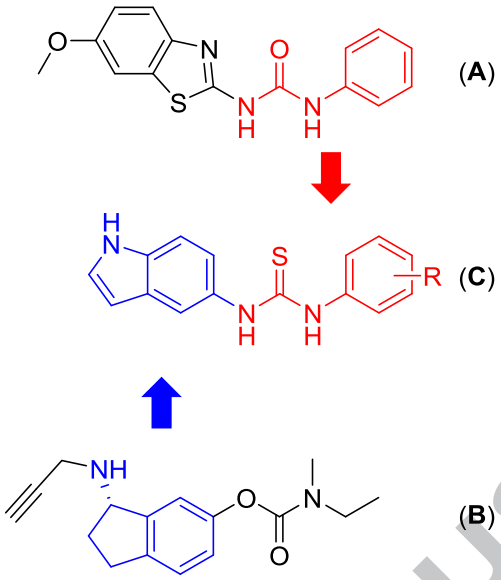

Fig. (1). Conjunctive design approach combining frentizole (**A**) and ladostigil (**B**) to novel MAO/ABAD inhibitors (**C**).

In this study we report the synthesis and *in vitro* evaluation of a novel series of these indolyl thiourea compounds. *In vitro* evaluation includes the inhibition of the MAO-A, MAO-B and ABAD enzymes in direct assays. The inhibition of horseradish peroxidase (HRP, used in the coupled assay for MAO activity) was also evaluated, but this inhibition was identified as a confounding factor in the initial evaluation of the novel compounds. Acute toxicity was determined via the MTT assay using the CHO-K1 cell line and the most promising compounds were selected for a PAMPA assay to evaluate their ability to cross the blood-brain-barrier (BBB).

2. Results

2.1. Chemistry

A two-step synthesis was performed to generate the desired disubstituted indolyl thioureas **3-23.** Electron-rich aromatic amines were readily converted to the corresponding isothiocyanates (Scheme 1, conditions a),[44] whereas electron poor aromatic amines required stronger basic conditions (Scheme 1, conditions b) to achieve conversion of the amine to a dithiocarbamic salt with following isothiocyanate (**2**) formation.[44,45] The isothiocyanates (**2**) were coupled with 1*H*-indol-5-amine to generate the disubstituted thioureas **3-23** (Table 1) in moderate to excellent yields (38-99%).[46] The reverse process with conversion of 1*H*-indol-5-amine to isothiocyanate and subsequent coupling step (Scheme 1, conditions d) with the second amine was used for final compounds with free phenolic group, where complete conversion to dithiocarbamic salt does not proceed quantitatively within reasonable time period. However, the outlined process in Scheme 1 was favoured due to higher reactivity of amines in the coupling step (Scheme 1,

conditions d), resulting in higher overall yields. The procedure also allowed compounds to be more readily purified by subsequent column chromatography rendering final compounds (**3-23**). The experimental section gives a detailed description of which procedure was used for each amine.

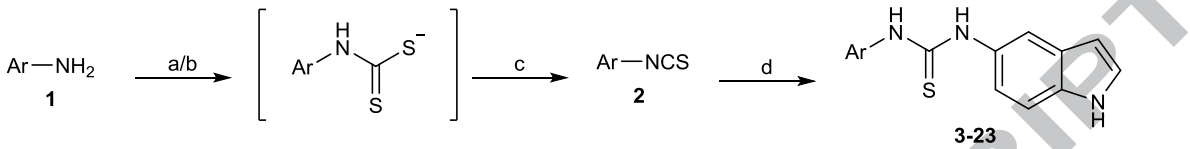

Scheme 1. Synthesis of indolyl thioureas **3-23**. Reagents and conditions: (a) CS_2, Et_3N, r.t. (b) NaH, CS_2, reflux; (c) Boc_2O, DMAP, 0°C to r.t.; (d) 1*H*-indole-5-amine, DCM, r.t.

Table 1. Substitution pattern and isolated yields of indolyl thioureas (**3-23**).

Comp.	Ar	Yield (%)	Comp.	Ar	Yield (%)	Comp.	Ar	Yield (%)
3	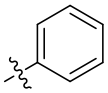	90	**10**	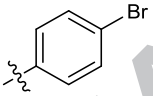	93	**17**	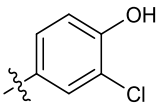	85
4	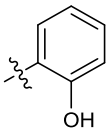	61	**11**	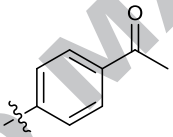	99	**18**	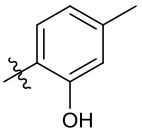	99
5	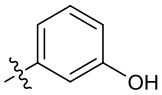	92	**12**	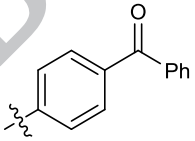	89	**19**	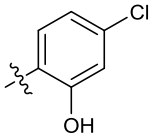	38
6	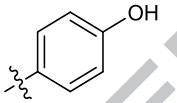	92	**13**	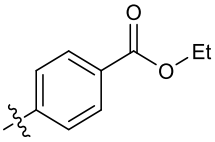	99	**20**	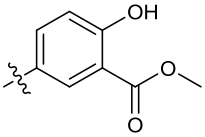	99
7	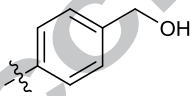	84	**14**	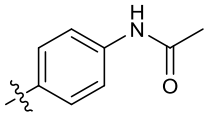	80	**21**	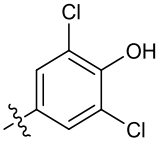	66
8	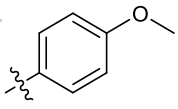	99	**15**	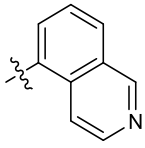	97	**22**	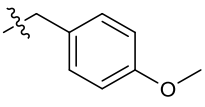	90
9	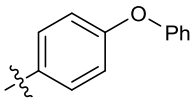	89	**16**	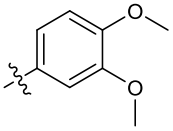	99	**23**	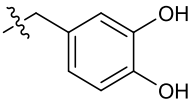	93

2.2. Biological activity

2.2.1. Controls in the coupled assay for MAO reveal HRP inhibition

An initial screen using a coupled fluorescence assay to assess MAO inhibition by the novel indole thiourea compounds suggested potent inhibition in the micromolar range that was not replicated in the direct spectrophotometric assay. The coupled assay uses HRP to detect the second MAO product, H_2O_2, resulting in the conversion of 10-acetyl-3,7-dihydroxyphenoxazine to resorufin.[47–49] The compounds did not quench the fluorescence of resorufin but most of them inhibited HRP by greater than 30% at 50 µM, the most potent by >80%. The inhibition of HRP by each compound at 5 or 50 µM is given as Supplementary Information (Table S1). The most potent HRP inhibitors, all with IC_{50} values of around 1 µM, always possessed a phenolic group, either in the 4-position (**6**, **17**, **21** and **23**) or 2-position (**4**) of the phenyl ring. The phenolic group has previously been associated with HRP inhibition, however on a flavonoid scaffold.[50] In light of these findings, we point out a potential flaw of the coupled Ampliflu™ Red assay, which may produce false positive results. In this study, the HRP inhibition at 1 µM prevented the use of the coupled assay to evaluate MAO inhibition.

2.2.2. Monoamine oxidase activity

To avoid the observed interference issues with the coupled assay, all compounds were evaluated using the kynuramine spectrophotometric assay.[51] All compounds were soluble in assay buffer at 100 µM but absorbed light at the wavelength (314 nm) of the kynuramine assay, limiting the maximum concentration to 30 µM for the initial screen. Compounds selected for further study could be used up to 100 µM. IC_{50} values were measured for all compounds using purified MAO-A as shown in Table 2. Several compounds displayed moderate to low micromolar range of inhibition, allowing selection of compounds for evaluation against membrane-bound MAO-A and MAO-B. IC_{50} values for the selected compounds are given in Table 2. The selectivity index calculated based on the IC_{50} values showed a small selectivity for MAO-B (**6, 15, 17, 18** and **19**).

2.2.3. ABAD activity

Compounds **3-23** were screened at a fixed 100 µM concentration to evaluate their inhibitory effect on ABAD activity with modified spectrophotometric assay.[26] The majority of the compounds did not significantly inhibit ABAD function. However, compounds **17** and **21** induced a decrease in ABAD activity of 51% or 61%, respectively (Table 2). Both compounds possess a phenolic group, which appears to be a key feature for displaying inhibition of ABAD. Based on the small effects observed in the 100 µM screen, the determination of IC_{50} was not possible since the concentration range needed would exceed the limits of assay.

Table 2. *In vitro* and cytotoxicity data for compounds **3-23**.

Compound	Ar	pure MAO-A IC_{50} (μM) [a]	mb MAO-A IC_{50} (μM) [b]	mb MAO-B IC_{50} (μM) [b]	ABAD 100 μM [c]	MTT LC_{50} (μM) [d]
frentizole	-	None	None	None	-	31 ± 3
3	Ph	> 30	57.5 ± 12	60 ± 12	85.8 ± 0.5	337 ± 0
4	2-OH-Ph	39 ± 19	14 ± 2	4.0 ± 0.8	85.0 ± 0.8	509 ± 10
5	3-OH-Ph	None	-	-	91.6 ± 0.6	977 ± 7
6	4-OH-Ph	None	> 100	17 ± 2	90.9 ± 0.6	848 ± 150
7	4-$OHCH_2$-Ph	None	-	-	84.2 ± 0.5	1080 ± 56
8	4-MeO-Ph	36 ± 15	36 ± 10	37 ± 11	91.3 ± 0.6	476 ± 28
9	4-PhO-Ph	None	-	-	90.9 ± 1.6	36 ± 10
10	4-Br-Ph	5.9 ± 1.3	23 ± 3	58 ± 12	83.0 ± 0.5	220 ± 43
11	4-MeCO-Ph	67	-	-	79.2 ± 0.9	154 ± 12
12	4-PhCO-Ph	None	-	-	80.4 ± 0.6	20 ± 2
13	4-COOEt-Ph	71	-	-	74.6 ± 1.0	123 ± 6
14	4-MeCONH-Ph	71	70 ± 13	37 ± 8	93.0 ± 1.0	1040 ± 30
15	isoquinolin-5-yl	24 ± 5	24 ± 4	4.0 ± 1.1	96.5 ± 0.8	> 400
16	3,4-MeO-Ph	None	-	-	93.8 ± 0.9	797 ± 116
17	3-Cl-4-OH-Ph	58 ± 18	58 ± 13	8.6 ± 1.2	49.1 ± 0.5	447 ± 2
18	2-OH-4-Me-Ph	None	24 ± 2	3.2 ± 0.7	87.2 ± 1.2	370 ± 30
19	2-OH-4-Cl-Ph	39 ± 9	6.3 ± 0.7	0.30 ± 0.12	76.0 ± 0.8	251 ± 2
20	3-COOMe-4-OH-Ph	None	> 100	31 ± 4	90.0 ± 0.8	423 ± 69
21	3,5-Cl-4-OH-Ph	None	> 100	17 ± 1	39.0 ± 0.6	523 ± 7
22	4-MeO-Bn	None	-	-	88.5 ± 1.2	232 ± 10
23	3,4-OH-Bn	None	-	-	81.5 ± 0.8	471 ± 73
amph.[53]	-	17.2 ± 0.2	5.33 ± 0.6	176 ± 45	-	-

[a] Each IC_{50} value (± SE of the estimate) comes from 8-12 individual spectrophotometric assays using purified human MAO-A. The maximum concentration used was 30 μM. Projected IC50 values above 30 μM are shown without error bars, but are given to allow the distinction from those compounds that showed no inhibition (None).
[b] Each IC_{50} value (± SE of the estimate) comes from 8-10 individual spectrophotometric assays using membrane-bound (mb) human MAO-A or MAO-B. The maximum concentration used was up to 100 μM.
[c] The values are expressed in percentage of remaining enzyme activity ± SEM (values are an average of two biological repeats each with three technical repeats).
[d] The LC_{50} value refers to 3 independent measurements ± SEM.

2.2.4. Cytotoxicity

To evaluate acute cytotoxicity, all compounds were screened using the standard MTT assay with the CHO-K1 cell line which is commonly used for cytotoxicity screening.[52] The observed toxicity was expressed as LC_{50} values (Table 2). The majority of the compounds showed very low levels of toxicity with an LC_{50} value over 200 µM compared to parent frentizole, producing valuable results for further investigation. Two compounds (**9** and **12**) showed elevated toxicity (LC_{50} ~20-40 µM) but these compounds didn't show any beneficial biological activity.

2.2.5. Blood-brain barrier permeation and physicochemical properties

Penetration across the BBB is an essential property for compounds targeting the CNS. In order to predict passive blood-brain penetration of most promising compounds prepared in the current study (**10**, **17**, **21**), a modification of the parallel artificial membrane permeation assay (PAMPA) has been used based on reported protocol.[54] The penetration value (P_e) was derived mathematically from time-dependent changes of the selected compounds' concentrations in two aqueous phases separated by the artificial membrane (see Experimental section). Compounds **10** and **17** showed P_e values greater than 4, which indicate sufficient passive transition of the compounds through the BBB (Table 3).[55,56]

For the physicochemical properties, the number of hydrogen bond donors (HBD), number of hydrogen bond acceptors (HBA), topological polar surface area (TPSA), logarithm of the *n*-octanol-water partition coefficient for non-ionized species (Clog*P*) and the *n*-octanol-water distribution coefficient (Clog*D*) reflecting the ratio of the ionic forms at pH = 7.4 have been calculated in ACDLabs PhysChem Suite 12.0 and compared with the experimental values of P_e and chromatographic capacity factors *k*. The three compounds **10**, **17** and **21** do not violate any of the Lipinski's rules of five, although P_e values (Table 4) apparently follow their own trend showing somewhat ambiguous relationship with *k* and the *in silico* molecular descriptors. The most striking deviation is exhibited by compound **21** that has a low penetration rate P_e despite its sufficient hydrophobicity as implied by relatively high values of Clog*P*, Clog*D* and *k*. This finding may results from overall physicochemical effect of 3,5-dichloro-4-hydroxy aromatic moiety (see Table 1) which renders **21** the most ionisable compound at the physiological pH of 7.4 in comparison to **10** and **17**. Therefore, it should be noted that the PAMPA (predictive) assay cannot be simplified by high performance liquid chromatography analysis or basic molecular descriptors (HBD/HBA, TPSA, Clog*P*/*D*), but it can be replaced *in vivo* experiments when the predicted values should be verified.

Table 3. Physical chemical properties of selected compounds.

Comp.	P_e ± SEM[a]	*k* ± SEM[b]	HBD/HBA[c]	TPSA[c]	Clog*P*[c]	Clog$D_{7.4}$[c]
10	6.9 ± 0.6	4.355 ± 0.000	3/3	71.9	3.57	3.57
17	7.3 ± 0.2	3.760 ± 0.000	4/4	92.2	3.16	3.12
21	3.0 ± 0.3	3.975 ± 0.000	4/4	92.2	4.14	3.61

[a] Prediction of blood-brain barrier penetration of drugs expressed as P_e ± SEM (*10^{-6} cm.s^{-1}). High BBB permeation predicted for P_e > 4; BBB permeation uncertain for P_e between 2.0 and 4.0; low BBB permeation predicted for < 2.0
[b] Capacity factors *k* determined by a gradient HPLC method on a reverse C18 stationary phase working in acid polar organic mode (pH ~3.5). The values of *k* given as mean ± SEM of 24 measurements.
[c] Calculated in ACDLabs PhysChem Suite 12.0

2.3. Molecular modelling

A molecular docking study was performed in an attempt to identify the binding modes of compound **19** within the MAO-A and MAO-B active sites. Flexible docking was performed using AutoDock Vina 1.1.2 and the 2Z5X (i.e. MAO-A) and 2V5Z (i.e. MAO-B) protein X-ray structures from the Protein Databank. Figure 2 shows the top-scored docking pose of compound **19** (-10.3 kcal/mol) located within the MAO-A cavity. Compound **19** was predicted to bind below the flavin moiety of the FAD cofactor. The indole five-membered ring of **19** displays alignment with Tyr407 phenyl ring supporting the formation of π-π stacking interaction (3.8 Å). The orientation of the *N*-indole hydrogen towards oxygen of Tyr444 phenolic group suggests further indole ring stabilization via hydrogen bonding (2.1 Å). A secondary weak hydrogen bond may also be formed between the thiourea nitrogen and amid hydrogen of Gln215 which are in near proximity (2.2 Å). Lastly, the distant 4-chloro-2-hydroxyphenyl ring of **19** is oriented towards the aromatic cycle of Phe208 suggesting the potential for a weak T-shaped π-π interaction (3.9 Å), where the para positioned chlorine points to a hydrophobic cavity formed by Leu97, Ala111 and Ile325 (pocket surface not shown for clarity of the figure). More or less similar interactions were revealed in the top-scored mode of compound **19** within the active site of MAO-B (-10.3 kcal/mol) (Fig. 3). In contrast to MAO-A, the indole moiety of **19** was stacked between Tyr435 (3.9 Å) and Tyr398 (3.7 Å) without involvement of the indole hydrogen in any polar interactions. Interestingly, the 2-hydroxy moiety of **19** was stabilized by H-bond interactions with hydroxyl of Tyr326 (2.5 Å) and terminal amide hydrogen of Gln206 (2.9 Å). Although the best docking scores of compound **19** in MAO-A/B do not suggest any significant binding preference for either of the enzymes, the calculations provided 9 energetically similar binding modes of compound **19** in MAO-B cavity, whilst in MAO-A cavity only 2 binding modes were found. However, the reason for the lack of thermodynamic explanation for the different IC_{50} values for MAO-A and MAO-B is still not obvious. Compounds can often bind with either end of the molecule close to the flavin in MAO,[57] or in rotated configuration.[58] In the latter article, molecular dynamics were used to understand a change in affinity, but that is beyond the scope of this exploratory study for these relatively weak inhibitors of MAO.

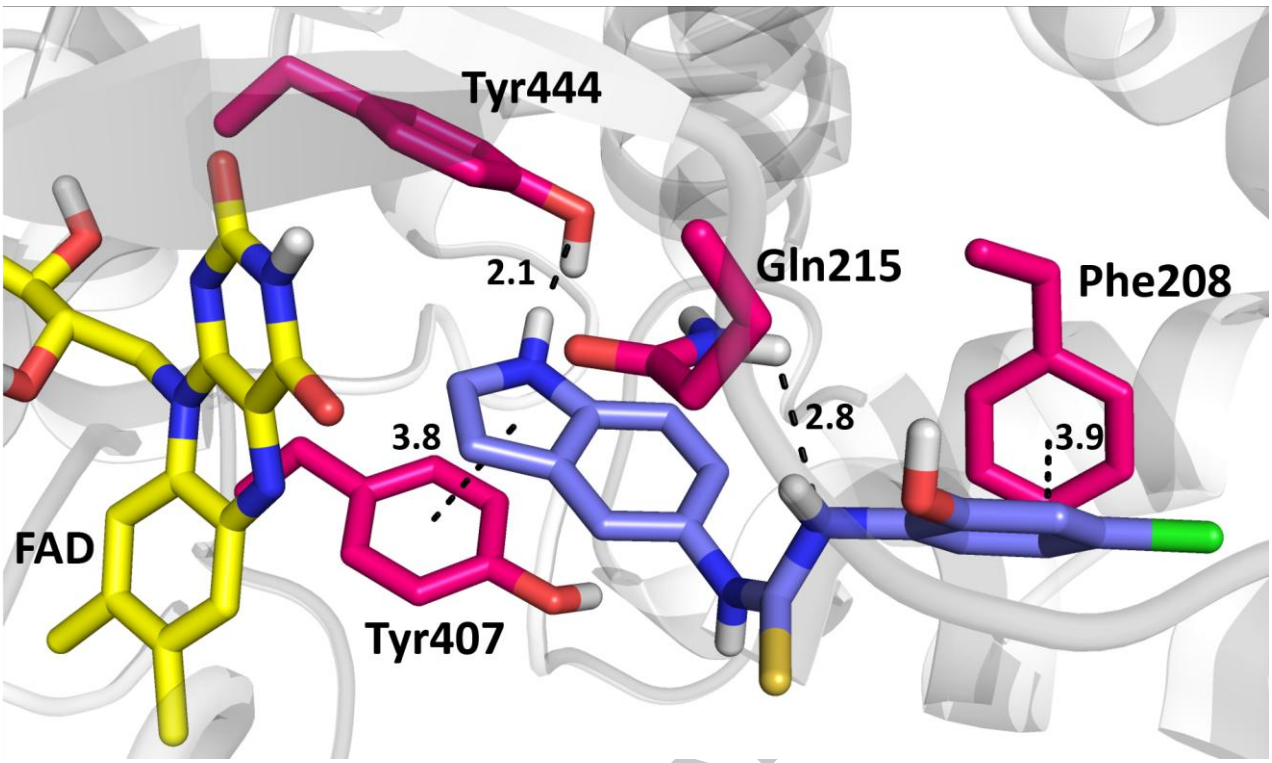

Fig. (2). Superimposition of **19** (-10.3 kcal/mol) in the active site MAO-A (PDB ID: 2Z5X). The ligand is shown as blue sticks, selected MAO-A residues as magenta sticks, flavin cofactor as yellow sticks and the backbone as light grey cartoon. For the sake of clarity, only four of residues are displayed.

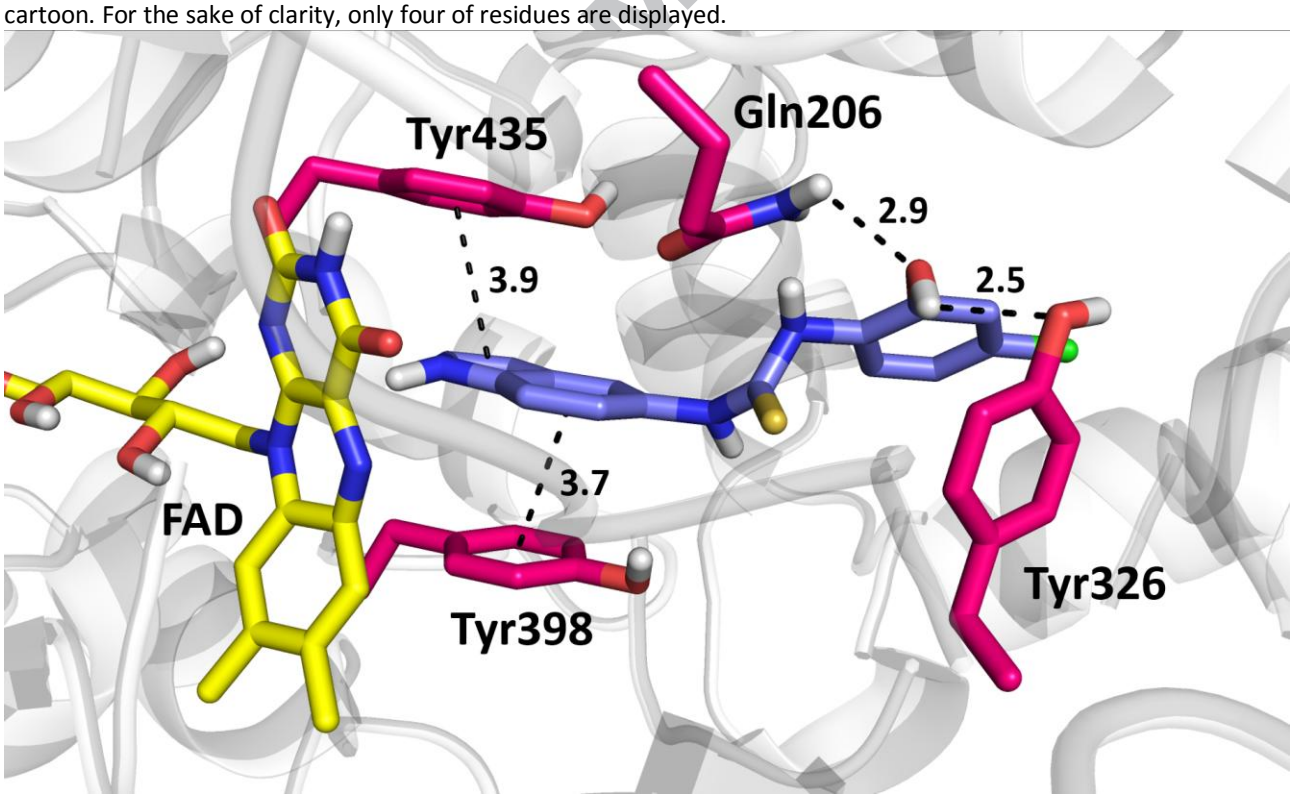

Fig. (3). Superimposition of **19** (-10.3 kcal/mol) in the active site MAO-B (PDB ID: 2V5Z). Ligand is shown as blue sticks, selected MAO-B residues as magenta sticks, flavin cofactor as yellow sticks and the backbone as light grey cartoon. For the sake of clarity, only four of residues are displayed.

3. Structure-activity relationship

Initial evaluation of the compounds on the activity of purified MAO-A identified only compound **10** (*para*-Br) as giving significant inhibition, with an IC_{50} value of 5.9 μM for purified human MAO-A, but several other (mainly para) substitutions were found on μM level (**4, 8, 15, 17, 19**). On the other hand, the introduction of a second phenyl ring connected via an ether (**9**) or a carbonyl moiety (**12**) resulted in the loss of activity, indicating the space limitation for the favoured *para* substituent. In contrast, isoquinolin-5-yl moiety (**15**) displayed promising inhibition.

For the selected compounds studied on both membrane-bound MAO-A and B, non-selective inhibition was observed only for the parent compound **3** (IC_{50} around 60 μM), and with the *para*-methoxy substituent **8** (IC_{50} around 36 μM). All other compounds were more selective for MAO-B. MAO-A inhibition was retained for *ortho*-hydroxyl-containing compounds (**4**, **19**) particularly with additional chlorine in the *para* (**19**) or *meta* position (**17**, **19**) and also for small lipophilic substitutions such as methoxy moiety (**8**), although with higher IC_{50}. The substituents generally improved inhibition of MAO-B. In the *para* position, the hydroxy moiety improved inhibition of MAO-B by 4-fold (**17** versus **3**). The *ortho* hydroxyl (**4**) improved binding to MAO-B by 15-fold (compared to only 4-fold on MAO-A) giving an IC_{50} decrease to 4 μM. With the *ortho*-hydroxyl present, *para* substitution with chlorine improved MAO-B inhibition to 0.3 μM (**19**), 10-fold better than a methyl substituent (**18**). In contrast, the *para* bromine moiety was favoured for MAO-A but not MAO-B inhibition (**10** versus **3**).

For inhibition of ABAD activity, compounds **17** and **21** were the most potent with a 4-hydroxy substitution and additionally chlorine on the distal phenyl ring. The 4-hydroxy moiety alone (**6)** gave inhibition comparable with other positioned isomers (**4** and **5**) and not much better than **3** without the hydroxyl group. The introduction of chlorine into the C-3 position (**17**) increased the inhibitory effect. Additionally, a second chlorine present in the C-5 position (**21**) further increased the inhibitory effect, which is in agreement with recently reported findings.[41] Functional groups other than chlorine (**20** and **23**) were not beneficial. Comparing the discussed compounds with the previously published urea/thiourea/phosphonate series, it shows that the inhibition ability doesn't vary significantly with the linker changes.[38–40] On the other hand, the bicyclic aromatic scaffold using substituted benzothiazole or other moiety might be a crucial factor. In this case, the introduction of indole moiety seems to be rather unfavourable for ABAD inhibitory ability if compared to previously used benzothiazoles.[38–41] This fact might be related to either its flipped position and/or missing substitution of the indolyl scaffold, which will be the matter of further investigation.

Taken together, the best MAO and ABAD inhibitors from presented series of compounds do not possess the same structural features required for inhibition of both enzymes, when ABAD inhibition seems to be restricted to the 3-chlorine-4-hydroxy or 3,5-chlorine-4-hydroxy scaffold. The presence of the phenolic moiety particularly influenced the activity on the MAO targets. An improved MAO inhibitory ability

(with a degree of MAO-B selectivity) was shown in a decrease of IC_{50} with presence of *ortho*-hydroxy group (**3** versus **4**), with an additional *para*-substitution with chlorine pushing the IC_{50} to low micromolar (MAO-A) and high nanomolar values (MAO-B) for compound **19**. In contrast, the most active ABAD inhibitors have the phenolic group restricted to the *para*-position of the distal phenyl ring, with improvement due to *meta*-substitution (single or double chlorine moiety).

Importantly, the majority of the tested MAO/ABAD inhibitors shared a low cytotoxic profile (usually one order of magnitude better) compared to parent compound frentizole. Only two compounds (**9** and **12**) showed higher cytotoxicity, possibly associated with their increased lipophilicity, since they contain an additional phenyl ring connected via ether or carbonyl linker. However, compounds **9** and **12** did not show biological activity valuable for further investigation.

4. Conclusion

In summary, a novel class of disubstituted thioureas was synthesized and evaluated for MAO-A, MAO-B and ABAD inhibitory ability and a cytotoxicity profile. Some compounds showed MAO inhibitory activity in the micromolar range (mostly with modest MAO-B selectivity), expanding the pool of known MAO inhibitors scaffolds. In case of ABAD, the molecular design was only partially successful in retaining ABAD inhibitory ability, with only two compounds showed promising structural features for ABAD inhibition. The majority of the compounds also exhibited HRP inhibitory properties, demonstrating the limitations for the use of the HRP-coupled assay, particularly with compounds possessing phenolic groups. Therefore, we emphasize caution when using coupled enzymatic reactions such as the Amplex™/Ampliflu™ Red assay, and the need to validate positive results with direct or different assays to avoid misconceptions in data interpretation.

Conflict of interest

The authors confirm that this article content has no conflict of interest.

Acknowledgement

This work was supported by the Ministry of Health of the Czech Republic (no. NV15-28967A), the Charles University in Prague (SVV 260 291), COST Action CM1103 (STSM 15879 and 17487) and CA15135, University of Hradec Kralove (Faculty of Informatics and Management, project Excellence 2015), University of St Andrews (undergraduate project funding to D.Z.), Biotechnology and Biological Sciences Research Council (BBSRC; no. BB/J01446X/1), the Alzheimer's Society and the Barcopel Foundation.

5. Experimental section

5.1. Synthesis

5.1.1. Chemicals and instrumentation

All reagents and solvents were purchased from commercial sources (Sigma Aldrich, Merck) and they were used without any further purification. Thin-layer chromatography for reaction monitoring was performed on Merck aluminium sheets, silica gel 60 F_{254}. NMR spectra (^{1}H and ^{13}C) were acquired at 500/125 MHz on a Varian S500 spectrometer or at 300/75 MHz on a Varian Gemini 300 spectrometer. Chemical shifts δ are given in ppm and referenced to the signal center of solvent peaks DMSO-d_6 (δ 2.50 ppm and 39.52 ppm for ^{1}H and ^{13}C, respectively). Coupling constants are expressed in Hz. High resolution mass spectra (HRMS) were recorded by coupled LCMS system consisting of Dionex UltiMate 3000 analytical LC system and Q Exactive Plus hybrid quadrupole-orbitrap spectrometer. As an ion-source, heated electro-spray ionization (HESI) was utilized (setting: sheath gas flow rate 40, aux gas flow rate 10, sweep gas flow rate 2, spray voltage 3.2 kV, capillary temperature 350°C, aux gas temperature 300°C, S-lens RF level 50. Positive ions were monitored in the range of 100-1500 m/z with the resolution set to 140 000. Obtained mass spectra were processed in Xcalibur 3.0.63 software. Uncalibrated purity > 95% at 254nm was confirmed for all the studied compounds by HPLC. Elemental analyses were carried out with CE Instruments EA-1110 CHN (CE Instruments, Wigan, UK). Melting points were determined on a Stuart SMP30 melting point apparatus and are uncorrected.

*5.1.2. General procedure for the synthesis of isothiocyanates for electron rich aromatic amines (**2**).*

This procedure was employed to generate corresponding isothiocyanates for final thioureas **3**-**9** and **14-23**. The reverse process, where 1*H*-indole-5-isothiocyanate was firstly generated followed by subsequent coupling with corresponding amine, was used for final thioureas with free phenolic groups (**4-7**, **17**, **19**, **21** and **23**).

An amine (**1**; 3 mmol) was dissolved in THF (5 mL). While stirring, CS_2 (30 mmol, 2.28 g, 1.80 mL) and Et_3N (3 mmol, 0.30 g, 0.42 mL) were added. After the complete conversion to dithiocarbamic acid salt (monitored via TLC, generally within 30-60 min), the reaction mixture was cooled on an ice bath with immediate addition of Boc_2O (2.97 mmol, 0.65 g, 1 mL THF solution) and DMAP (0.03 mmol, 11 mg, 0.5 mL THF solution). Complete consumption of dithiocarbamic acid salt proceeded within 15-60 min. Solvent and other volatiles were removed under reduced pressure yielding isothiocyanate (**2**) quantitatively (TLC) and used in next step without further purification.[44]

*5.1.3. General procedure for the synthesis of isothiocyanates electron poor aromatic amines (**2**).*

This procedure was employed to generate corresponding isothiocyanates for final thioureas **10**-**13**.

An amine (**1**; 3 mmol) was dissolved in THF (10 mL) and cooled on an ice bath. NaH (60% in mineral oil; 1.5 mmol, 0.18 g) was added and mixture was stirred for next 10 min on an ice bath. CS_2 (9 mmol, 0.69 g, 0.54 mL) was added drop-wise and the reaction was allowed to reach room temperature. The mixture was refluxed for 18 h and then cooled on an ice bath. Boc_2O (2.97 mmol, 0.65 g, 1 mL THF solution) and DMAP (0.03 mmol, 11 mg, 0.5 mL THF solution) were added. The mixture was stirred for next 60 min at room temperature. The solution was acidified with 1 N HCl (15 mL) and extracted with Et_2O (3×20 mL). The combined organic layers were dried (Na_2SO_4) and the solvent was removed under reduced pressure. The residue was purified by column chromatography (silica gel, heptane-EtOAc, 5:1) to afford isothiocyanate (**2**), which was directly used in next step.[44,45]

*5.1.4. General procedure for the synthesis of 1-aryl-3-(1H-indol-5-yl)thiourea (**3-23**):*

The aromatic amine (1 mmol) was dissolved in DCM (5 mL). Solution of isothiocyanate (1 mmol) in DCM (2 mL) was added drop-wise and the mixture was stirred for 20 h at room temperature.[46] Solvent was removed under reduced pressure and the residue was purified by column chromatography (silica gel, $CHCl_3$-MeOH) to yield corresponding product. Compounds were recrystallized from Et_2O-EtOAc to yield final thiourea.

1-(1*H*-indol-5-yl)-3-phenylthiourea (**3**)

Light-yellow solid, yield 0.24 g (90%), mp 159-160 °C. ^{1}H NMR (500 MHz, DMSO-d_6) δ 11.10 (s, 1H), 9.67 (s, 1H), 9.45 (s, 1H), 7.55 (d, *J* = 1.5 Hz, 1H), 7.50 (d, *J* = 7.5 Hz, 2H), 7.39 – 7.34 (m, 2H), 7.33 – 7.28 (m, 2H), 7.13 – 7.05 (m, 2H), 6.45 – 6.40 (m, 1H). ^{13}C NMR (125 MHz, DMSO-d_6) δ 179.96, 139.81, 133.88, 130.54, 128.21, 127.53, 126.06, 124.12, 123.78, 119.47, 116.40, 111.23, 101.28. HRMS (HESI) calcd for $C_{15}H_{14}N_3S$ $[M+H]^+$ 268.09029, found 268.09042. Anal. calcd for $C_{15}H_{13}N_3S$: C, 67.39; H, 4.90; N, 15.72; S, 11.99. Found C, 67.15; H, 5.04; N, 15.49; S, 12.05.

1-(2-hydroxyphenyl)-3-(1*H*-indol-5-yl)thiourea (**4**)

Beige solid, yield 0.17 g (61%), mp 137-138 °C. ^{1}H NMR (300 MHz, DMSO-d_6) δ 11.15 (s, 1H), 9.86 (s, 1H), 9.75 (s, 1H), 8.76 (s, 1H), 8.14 (d, *J* = 7.7 Hz, 1H), 7.58 (s, 1H), 7.45 – 7.32 (m, 2H), 7.08 (d, *J* = 8.5 Hz, 1H), 6.99 – 6.89 (m, 1H), 6.87 – 6.71 (m, 2H), 6.44 (s, 1H). ^{13}C NMR (75 MHz, DMSO-d_6) δ 178.95, 148.80, 134.04, 129.96, 127.66, 127.14, 126.29, 124.81, 124.25, 119.56, 118.41, 116.71, 115.09, 111.53, 101.35. HRMS (HESI) calcd for $C_{15}H_{14}N_3OS$ $[M+H]^+$ 284.08521, found 284.08502. Anal. calcd for $C_{15}H_{13}N_3OS$: C, 63.58; H, 4.62; N, 14.83; S, 11.31. Found C, 63.25; H, 4.88; N, 14.51; S, 11.27.

1-(3-hydroxyphenyl)-3-(1*H*-indol-5-yl)thiourea (**5**)

Off-white solid, yield 0.26 g (92%), mp 102-104 °C. ^{1}H NMR (500 MHz, DMSO-d_6) δ 11.08 (s, 1H), 9.57 (s, 1H), 9.39 (s, 2H), 7.54 (d, *J* = 1.6 Hz, 1H), 7.38 – 7.33 (m, 2H), 7.11 – 7.05 (m, 2H), 7.04 (t, *J* = 2.1 Hz, 1H), 6.87 (dd, *J* = 8.0, 1.1 Hz, 1H), 6.53 – 6.49 (m, 1H), 6.44 – 6.40 (m, 1H). ^{13}C NMR (125 MHz, DMSO-d_6) δ

179.69, 157.32, 140.71, 133.83, 130.71, 129.00, 127.48, 126.02, 119.53, 116.37, 114.00, 111.26, 111.12, 110.42, 101.26. HRMS (HESI) calcd for $C_{15}H_{14}N_3OS$ $[M+H]^+$ 284.08521, found 284.08505. Anal. calcd for $C_{15}H_{13}N_3OS$: C, 63.58; H, 4.62; N, 14.83; S, 11.31. Found C, 63.23; H, 4.55; N, 14.56; S, 11.02.

1-(4-hydroxyphenyl)-3-(1*H*-indol-5-yl)thiourea (**6**)

Off-white solid, yield 0.26 g (92%), mp 188-190 °C. ^{1}H NMR (500 MHz, DMSO-d_6) δ 11.07 (s, 1H), 9.40 (s, 1H), 9.30 (br s, 1H), 9.15 (s, 1H), 7.52 (d, *J* = 1.6 Hz, 1H), 7.37 – 7.32 (m, 2H), 7.22 – 7.15 (m, 2H), 7.05 (dd, *J* = 8.6, 2.0 Hz, 1H), 6.75 – 6.68 (m, 2H), 6.44 – 6.39 (m, 1H). ^{13}C NMR (125 MHz, DMSO-d_6) δ 180.31, 154.70, 133.85, 130.86, 130.69, 127.52, 126.47, 126.00, 119.66, 116.53, 114.85, 111.17, 101.27. HRMS (HESI) calcd for $C_{15}H_{14}N_3OS$ $[M+H]^+$ 284.08521, found 284.08514. Anal. calcd for $C_{15}H_{13}N_3OS$: C, 63.58; H, 4.62; N, 14.83; S, 11.31. Found C, 63.29; H, 4.83; N, 14.61; S, 11.58.

1-(4-(hydroxymethyl)phenyl)-3-(1*H*-indol-5-yl)thiourea (**7**)

Light-brown solid, yield 0.25 g (84%), mp 151-152 °C. ^{1}H NMR (500 MHz, DMSO-d_6) δ 11.10 (s, 1H), 9.62 (s, 1H), 9.41 (s, 1H), 7.55 (s, 1H), 7.46 – 7.40 (m, 2H), 7.39 – 7.33 (m, 2H), 7.29 – 7.22 (m, 2H), 7.08 (dd, *J* = 8.6, 1.8 Hz, 1H), 6.43 (s, 1H), 5.14 (t, *J* = 5.7 Hz, 1H), 4.46 (d, *J* = 5.7 Hz, 2H). ^{13}C NMR (125 MHz, DMSO-d_6) δ 180.04, 138.48, 138.32, 133.89, 130.58, 127.54, 126.44, 126.07, 123.74, 119.53, 116.44, 111.24, 101.30, 62.64. HRMS (HESI) calcd for $C_{16}H_{16}N_3OS$ $[M+H]^+$ 298.10086, found 298.10074. Anal. calcd for $C_{16}H_{15}N_3OS$: C, 64.62; H, 5.08; N, 14.13; S, 10.78. Found C, 64.36; H, 5.04; N, 13.92; S, 11.02.

1-(1*H*-indol-5-yl)-3-(4-methoxyphenyl)thiourea (**8**)

Off-white solid, yield 0.30 g (99%), mp 157-158 °C. ^{1}H NMR (500 MHz, DMSO-d_6) δ 11.09 (s, 1H), 9.50 (s, 1H), 9.24 (s, 1H), 7.53 (d, *J* = 1.8 Hz, 1H), 7.39 – 7.30 (m, 4H), 7.06 (dd, *J* = 8.6, 1.8 Hz, 1H), 6.92 – 6.85 (m, 2H), 6.42 (s, 1H), 3.74 (s, 3H). ^{13}C NMR (125 MHz, DMSO-d_6) δ 180.29, 156.38, 133.86, 132.54, 130.59, 127.53, 126.18, 126.02, 119.57, 116.48, 113.46, 111.21, 101.26, 55.19. HRMS (HESI) calcd for $C_{16}H_{16}N_3OS$ $[M+H]^+$ 298.10086, found 298.10068. Anal. calcd for $C_{16}H_{15}N_3OS$: C, 64.62; H, 5.08; N, 14.13; S, 10.78. Found C, 64.40; H, 5.10; N, 13.98; S, 10.98.

1-(1*H*-indol-5-yl)-3-(4-phenoxyphenyl)thiourea (**9**)

Beige solid, yield 0.32 g (89%), mp 180-181 °C. ^{1}H NMR (500 MHz, DMSO-d_6) δ 11.10 (s, 1H), 9.64 (s, 1H), 9.42 (s, 1H), 7.53 (d, *J* = 1.1 Hz, 1H), 7.49 – 7.44 (m, 2H), 7.41 – 7.33 (m, 4H), 7.12 (t, *J* = 7.4 Hz, 1H), 7.06 (dd, *J* = 8.6, 1.9 Hz, 1H), 7.01 – 6.94 (m, 4H), 6.44 – 6.40 (m, 1H). ^{13}C NMR (125 MHz, DMSO-d_6) δ 180.13, 157.07, 152.97, 135.38, 133.89, 130.53, 129.97, 127.53, 126.06, 125.97, 123.15, 119.52, 118.66, 118.15, 116.47, 111.23, 101.27. HRMS (HESI) calcd for $C_{21}H_{18}N_3OS$ $[M+H]^+$ 360.11651, found 360.11618. Anal. calcd for $C_{21}H_{17}N_3OS$: C, 70.17; H, 4.77; N, 11.69; S, 8.92. Found C, 69.88; H, 4.96; N, 11.47; S, 9.19.

1-(4-bromophenyl)-3-(1*H*-indol-5-yl)thiourea (**10**)

Beige solid, yield 0.32 g (93%), mp 190-191 °C. ^{1}H NMR (500 MHz, DMSO-d_6) δ 11.11 (s, 1H), 9.78 (s, 1H), 9.52 (s, 1H), 7.53 (d, *J* = 1.4 Hz, 1H), 7.48 (s, 4H), 7.39 – 7.34 (m, 2H), 7.06 (dd, *J* = 8.6, 2.0 Hz, 1H), 6.44

– 6.41 (m, 1H). ^{13}C NMR (125 MHz, DMSO-d_6) δ 179.90, 139.33, 133.93, 130.94, 130.36, 127.54, 126.11, 125.73, 119.40, 116.41, 116.04, 111.29, 101.30. HRMS (HESI) calcd for $C_{15}H_{13}BrN_3S$ $[M+H]^+$ 346.00081, found 346.00082. Anal. calcd for $C_{15}H_{12}BrN_3S$: C, 52.03; H, 3.49; N, 12.14; S, 9.26. Found C, 52.13; H, 3.40; N, 12.25; S, 9.48.

1-(4-acetylphenyl)-3-(1*H*-indol-5-yl)thiourea (**11**)

Light-yellow solid, yield 0.33 g (99%), mp 163-164 °C. ^{1}H NMR (500 MHz, DMSO-d_6) δ 11.12 (s, 1H), 9.99 (s, 1H), 9.89 (s, 1H), 7.93 – 7.88 (m, 2H), 7.76 – 7.71 (m, 2H), 7.58 (s, 1H), 7.40 – 7.35 (m, 2H), 7.09 (dd, *J* = 8.6, 1.9 Hz, 1H), 6.45 – 6.41 (m, 1H), 2.54 (s, 3H). ^{13}C NMR (125 MHz, DMSO-d_6) δ 196.57, 179.59, 144.59, 133.94, 131.82, 130.40, 128.74, 127.51, 126.14, 121.66, 119.26, 116.24, 111.28, 101.31, 26.48. HRMS (HESI) calcd for $C_{17}H_{16}N_3OS$ $[M+H]^+$ 310.10086, found 310.10062. Anal. calcd for $C_{17}H_{15}N_3OS$: C, 66.00; H, 4.89; N, 13.58; S, 10.36. Found C, 66.25; H, 5.11; N, 13.43; S, 10.11.

1-(4-benzoylphenyl)-3-(1*H*-indol-5-yl)thiourea (**12**)

White solid, yield 0.33 g (89%), mp 198-199 °C. ^{1}H NMR (500 MHz, DMSO-d_6) δ 11.13 (s, 1H), 9.99 (s, 1H), 9.91 (s, 1H), 7.80 – 7.75 (m, 2H), 7.74 – 7.69 (m, 4H), 7.66 (t, *J* = 7.4 Hz, 1H), 7.60 – 7.53 (m, 3H), 7.41 – 7.35 (m, 2H), 7.10 (dd, *J* = 8.6, 1.4 Hz, 1H), 6.46 – 6.42 (m, 1H). ^{13}C NMR (125 MHz, DMSO-d_6) δ 194.58, 179.58, 144.38, 137.54, 133.95, 132.23, 131.51, 130.41, 129.34, 128.47, 127.52, 126.16, 121.65, 119.26, 116.25, 111.28, 101.32. HRMS (HESI) calcd for $C_{22}H_{18}N_3OS$ $[M+H]^+$ 372.11651, found 372.11627. Anal. calcd for $C_{22}H_{17}N_3OS$: C, 71.14; H, 4.61; N, 11.31; S, 8.63. Found C, 70.92; H, 4.67; N, 11.13; S, 8.32.

Ethyl 4-(3-(1*H*-indol-5-yl)thioureido)benzoate (**13**)

Off-white solid, yield 0.36 g (99%), mp 149-150 °C. ^{1}H NMR (500 MHz, DMSO-d_6) δ 11.12 (s, 1H), 9.94 (s, 1H), 9.82 (br s, 1H), 7.93 – 7.86 (m, 2H), 7.75 – 7.69 (m, 2H), 7.57 (s, 1H), 7.41 – 7.33 (m, 2H), 7.09 (dd, *J* = 8.6, 1.6 Hz, 1H), 6.46 – 6.41 (m, 1H), 4.29 (q, *J* = 7.1 Hz, 2H), 1.31 (t, *J* = 7.1 Hz, 3H). ^{13}C NMR (125 MHz, DMSO-d_6) δ 179.64, 165.38, 144.56, 133.96, 130.36, 129.50, 127.52, 126.15, 124.41, 121.92, 119.30, 116.31, 111.29, 101.32, 60.41, 14.22. HRMS (HESI) calcd for $C_{18}H_{18}N_3O_2S$ $[M+H]^+$ 340.11142, found 340.11133. Anal. calcd for $C_{18}H_{17}N_3O_2S$: C, 63.70; H, 5.05; N, 12.38; S, 9.45. Found C, 63.53; H, 5.12; N, 12.13; S, 9.68.

N-(4-(3-(1*H*-indol-5-yl)thioureido)phenyl)acetamide (**14**)

Beige solid, yield 0.26 g (80%), mp 172-174 °C. ^{1}H NMR (500 MHz, DMSO-d_6) δ 11.09 (s, 1H), 9.90 (s, 1H), 9.56 (s, 1H), 9.33 (s, 1H), 7.58 – 7.46 (m, 3H), 7.42 – 7.29 (m, 4H), 7.06 (d, *J* = 8.4 Hz, 1H), 6.42 (s, 1H), 2.03 (s, 3H). ^{13}C NMR (125 MHz, DMSO-d_6) δ 180.04, 168.05, 135.92, 134.71, 133.89, 130.58, 127.54, 126.05, 124.71, 119.58, 118.91, 116.50, 111.22, 101.29, 23.92. HRMS (HESI) calcd for $C_{17}H_{17}N_4OS$ $[M+H]^+$ 325.11176, found 325.11176. Anal. calcd for $C_{17}H_{16}N_4OS$: C, 62.94; H, 4.97; N, 17.27; S, 9.88. Found C, 62.71; H, 5.01; N, 16.99; S, 10.12.

1-(1*H*-indol-5-yl)-3-(isoquinolin-5-yl)thiourea (**15**)

Beige solid, yield 0.31 g (97%), mp 213-214 °C. ^{1}H NMR (300 MHz, DMSO-d_6) δ 11.13 (s, 1H), 9.85 (s, 1H), 9.61 (s, 1H), 9.33 (s, 1H), 8.55 (d, *J* = 5.6 Hz, 1H), 8.01 (d, *J* = 7.8 Hz, 1H), 7.89 – 7.74 (m, 2H), 7.72 – 7.56 (m, 2H), 7.46 – 7.30 (m, 2H), 7.15 (d, *J* = 8.1 Hz, 1H), 6.45 (s, 1H). ^{13}C NMR (75 MHz, DMSO-d_6) δ 181.64, 152.47, 142.78, 135.16, 134.09, 132.70, 130.47, 129.40, 128.96, 127.62, 127.14, 126.16, 125.92, 119.79, 116.95, 116.38, 111.39, 101.37. HRMS (HESI) calcd for $C_{18}H_{15}N_4S$ $[M+H]^+$ 319.10119, found 319.10117. Anal. calcd for $C_{18}H_{14}N_4S$: C, 67.90; H, 4.43; N, 17.60; S, 10.07. Found C, 67.67; H, 4.24; N, 17.33; S, 9.80.

1-(3,4-dimethoxyphenyl)-3-(1*H*-indol-5-yl)thiourea (**16**)

Off-white solid, yield 0.34 g (99%), mp 152.5-153.5 °C. ^{1}H NMR (500 MHz, DMSO-d_6) δ 11.09 (s, 1H), 9.49 (s, 1H), 9.27 (s, 1H), 7.52 (d, *J* = 1.6 Hz, 1H), 7.38 – 7.32 (m, 2H), 7.14 (d, *J* = 2.3 Hz, 1H), 7.06 (dd, *J* = 8.6, 2.0 Hz, 1H), 6.93 (dd, *J* = 8.6, 2.3 Hz, 1H), 6.89 (d, *J* = 8.6 Hz, 1H), 6.44 – 6.40 (m, 1H), 3.74 (s, 3H), 3.73 (s, 3H). ^{13}C NMR (125 MHz, DMSO-d_6) δ 180.04, 148.23, 146.01, 133.89, 132.72, 130.61, 127.52, 126.03, 119.66, 116.59, 116.54, 111.53, 111.19, 109.54, 101.27, 55.70, 55.47. HRMS (HESI) calcd for $C_{17}H_{18}N_3O_2S$ $[M+H]^+$ 328.11142, found 328.11111. Anal. calcd for $C_{17}H_{17}N_3O_2S$: C, 62.37; H, 5.23; N, 12.83; S, 9.79. Found C, 62.11; H, 5.37; N, 12.59; S, 10.01.

1-(3-chloro-4-hydroxyphenyl)-3-(1*H*-indol-5-yl)thiourea (**17**)

Light-brown solid, yield 0.27 g (85%), mp 152-153 °C. ^{1}H NMR (500 MHz, DMSO-d_6) δ 11.09 (s, 1H), 10.02 (s, 1H), 9.58 (s, 1H), 9.22 (s, 1H), 7.51 (d, *J* = 1.9 Hz, 1H), 7.44 (d, *J* = 2.5 Hz, 1H), 7.38 – 7.32 (m, 2H), 7.14 (dd, *J* = 8.7, 2.5 Hz, 1H), 7.04 (dd, *J* = 8.6, 1.9 Hz, 1H), 6.90 (d, *J* = 8.7 Hz, 1H), 6.45 – 6.40 (m, 1H). ^{13}C NMR (125 MHz, DMSO-d_6) δ 180.29, 150.25, 133.93, 131.84, 130.44, 127.56, 126.47, 126.07, 124.97, 119.59, 118.59, 116.59, 115.90, 111.27, 101.30. HRMS (HESI) calcd for $C_{15}H_{13}ClN_3OS$ $[M+H]^+$ 318.04624, found 318.04614. Anal. calcd for $C_{15}H_{12}ClN_3OS$: C, 56.69; H, 3.81; N, 13.22; S, 10.09. Found C, 56.91; H, 4.01; N, 12.95; S, 10.29.

1-(2-hydroxy-4-methylphenyl)-3-(1*H*-indol-5-yl)thiourea (**18**)

Light-yellow solid, yield 0.27 g (99%), mp 143.5-144.5 °C. ^{1}H NMR (500 MHz, DMSO-d_6) δ 11.13 (s, 1H), 9.74 (s, 1H), 9.60 (br s, 1H), 8.68 (br s, 1H), 7.89 (d, *J* = 7.9 Hz, 1H), 7.57 (s, 1H), 7.43 – 7.34 (m, 2H), 7.08 (dd, *J* = 8.6, 1.8 Hz, 1H), 6.65 (s, 1H), 6.58 (d, *J* = 8.2 Hz, 1H), 6.43 (s, 1H), 2.20 (s, 3H). ^{13}C NMR (125 MHz, DMSO-d_6) δ 179.03, 148.95, 134.35, 134.00, 130.08, 127.64, 126.23, 124.55, 124.48, 119.56, 119.05, 116.66, 115.79, 111.46, 101.32, 20.71. HRMS (HESI) calcd for $C_{16}H_{16}N_3OS$ $[M+H]^+$ 298.10086, found 298.10065. Anal. calcd for $C_{16}H_{15}N_3OS$: C, 64.62; H, 5.08; N, 14.13; S, 10.78. Found C, 64.48; H, 5.18; N, 13.89; S, 10.94.

1-(4-chloro-2-hydroxyphenyl)-3-(1*H*-indol-5-yl)thiourea (**19**)

Beige solid, yield 0.12 g (38%), mp 150-151 °C. ^{1}H NMR (500 MHz, DMSO-d_6) δ 11.14 (s, 1H), 10.31 (s, 1H), 9.93 (s, 1H), 8.76 (br s, 1H), 8.14 (d, *J* = 7.9 Hz, 1H), 7.58 (s, 1H), 7.47 – 7.31 (m, 2H), 7.08 (d, *J* = 7.8 Hz, 1H), 6.93 – 6.73 (m, 2H), 6.44 (s, 1H). ^{13}C NMR (125 MHz, DMSO-d_6) δ 179.12, 150.04, 134.05, 129.92, 128.12, 127.62, 126.42, 126.27, 125.58, 119.51, 118.11, 116.69, 114.75, 111.48, 101.33. HRMS (HESI) calcd

for $C_{15}H_{13}ClN_3OS$ $[M+H]^+$ 318.04624, found 318.04617. Anal. calcd for $C_{15}H_{12}ClN_3OS$: C, 56.69; H, 3.81; N, 13.22; S, 10.09. Found C, 56.44; H, 3.56; N, 13.39; S, 10.38.

Methyl 5-(3-(1*H*-indol-5-yl)thioureido)-2-hydroxybenzoate (**20**)

White solid, yield 0.35 g (99%), mp 137-138 °C. ^{1}H NMR (500 MHz, DMSO-d_6) δ 11.11 (s, 1H), 10.36 (s, 1H), 9.67 (s, 1H), 9.29 (s, 1H), 7.81 (d, *J* = 2.3 Hz, 1H), 7.57 (dd, *J* = 8.8, 2.5 Hz, 1H), 7.51 (s, 1H), 7.40 – 7.33 (m, 2H), 7.07 – 7.01 (m, 1H), 6.94 (d, *J* = 8.8 Hz, 1H), 6.43 (s, 1H), 3.89 (s, 3H). ^{13}C NMR (125 MHz, DMSO-d_6) δ 180.47, 168.93, 157.17, 134.00, 133.29, 131.58, 130.24, 127.61, 126.21, 126.10, 119.56, 116.92, 116.65, 112.18, 111.37, 101.31, 52.48. HRMS (HESI) calcd for $C_{17}H_{16}N_3O_3S$ $[M+H]^+$ 342.09069, found 342.09082. Anal. calcd for $C_{17}H_{15}N_3O_3S$: C, 59.81; H, 4.43; N, 12.31; S, 9.39. Found C, 59.68; H, 4.76; N, 12.02; S, 9.71.

1-(3,5-dichloro-4-hydroxyphenyl)-3-(1*H*-indol-5-yl)thiourea (**21**)

Beige solid, yield 0.22 g (66%), mp 174-175 °C. ^{1}H NMR (500 MHz, DMSO-*d6*) δ 11.11 (s, 1H), 9.94 (s, 1H), 9.79 (s, 1H), 9.34 (s, 1H), 7.50 (d, *J* = 0.9 Hz, 1H), 7.46 (s, 2H), 7.40 – 7.32 (m, 2H), 7.03 (dd, *J* = 8.6, 1.8 Hz, 1H), 6.44 – 6.40 (m, 1H). ^{13}C NMR (125 MHz, DMSO-d_6) δ 180.14, 145.94, 134.01, 132.68, 130.16, 127.59, 126.13, 124.89, 121.36, 119.50, 116.62, 111.37, 101.32. HRMS (HESI) calcd for $C_{15}H_{12}Cl_2N_3OS$ $[M+H]^+$ 352.00726, found 352.00729. Anal. calcd for $C_{15}H_{11}Cl_2N_3OS$: C, 51.15; H, 3.15; N, 11.93; S, 9.10. Found C, 51.41; H, 3.37; N, 11.68; S, 9.35.

1-(1*H*-indol-5-yl)-3-(4-methoxybenzyl)thiourea (**22**)

Beige solid, yield 0.28 g (90%), mp 155-156 °C. ^{1}H NMR (500 MHz, DMSO-d_6) δ 11.11 (s, 1H), 9.42 (s, 1H), 7.69 (br s, 1H), 7.44 (s, 1H), 7.39 – 7.33 (m, 2H), 7.25 (d, *J* = 8.5 Hz, 2H), 6.95 (dd, *J* = 8.5, 1.4 Hz, 1H), 6.88 (d, *J* = 8.5 Hz, 2H), 6.42 (s, 1H), 4.64 (d, *J* = 5.4 Hz, 2H), 3.73 (s, 3H). ^{13}C NMR (125 MHz, DMSO-d_6) δ 180.97, 158.16, 134.02, 131.38, 129.73, 128.66, 127.72, 126.17, 119.62, 116.84, 113.56, 111.60, 101.30, 55.03, 46.78. HRMS (HESI) calcd for $C_{17}H_{18}N_3OS$ $[M+H]^+$ 312.11651, found 312.11636. Anal. calcd for $C_{17}H_{17}N_3OS$: C, 65.57; H, 5.50; N, 13.49; S, 10.30. Found C, 65.29; H, 5.60; N, 13.37; S, 10.40.

1-(3,4-dihydroxybenzyl)-3-(1*H*-indol-5-yl)thiourea (**23**)

Light-brown solid, yield 0.29 g (93%), mp 50-51 °C. ^{1}H NMR (500 MHz, DMSO-d_6) δ 11.10 (s, 1H), 9.38 (s, 1H), 8.85 (br s, 1H), 8.71 (br s, 1H), 7.57 (br s, 1H), 7.45 (s, 1H), 7.39 – 7.31 (m, 2H), 6.96 (dd, *J* = 8.5, 1.8 Hz, 1H), 6.74 (d, *J* = 1.7 Hz, 1H), 6.66 (d, *J* = 8.0 Hz, 1H), 6.56 (dd, *J* = 8.0, 1.5 Hz, 1H), 6.42 – 6.38 (m, 1H), 4.54 (d, *J* = 5.1 Hz, 2H). ^{13}C NMR (125 MHz, DMSO-d_6) δ 180.83, 145.01, 144.16, 133.97, 130.09, 129.85, 127.70, 126.17, 119.58, 118.35, 116.72, 115.24, 114.99, 111.55, 101.30, 47.13. HRMS (HESI) calcd for $C_{16}H_{16}N_3O_2S$ $[M+H]^+$ 314.09577, found 314.09558. Anal. calcd for $C_{16}H_{15}N_3O_2S$: C, 61.32; H, 4.82; N, 13.41; S, 10.23. Found C, 61.05; H, 5.03; N, 13.12; S, 10.36.

5.2. In vitro evaluation

Ampliflu™ Red (10-acetyl-3,7-dihydroxyphenoxazine), kynuramine, horseradish peroxidase, human MAO-A and MAO-B (expressed in insect cell membranes) were purchased from Sigma-Aldrich. Human MAO-A from heterologous expression in yeast was purified as previously reported.[51] Compounds were dissolved in DMSO and stored in glass vials at 4°C in the dark. Control and inhibitor assays contained the same amount of DMSO (1% (v/v)). A multi-mode microplate reader (Molecular Devices FilterMax F5) was used for fluorometric assays with HRP and Ampliflu™ Red. A Uvikon 2101 spectrophotometer was used for absorbance assays with MAO-A and MAO-B. The IC_{50} values for selected compounds were determined by plotting remaining activity of enzyme against the log of compound concentration. Data analysis was performed with GraphPad Prism 5 software using the three parameter equation.

5.2.1. Fluorescence quenching and horseradish peroxidase activity assay

No fluorescence quenching of resorufin (1 µM and 10 µM) was observed in the presence of tested compounds (50 µM). Additionally, an inhibitory effect on HRP was evaluated using modified Ampliflu™ Red, where a direct HRP substrate (H_2O_2) was used instead of *in-situ* MAO-generated H_2O_2.[47,49,59] The assay mixture with a final volume of 200 µL 50 mM potassium phosphate buffer (pH 7.4) in the well contained; H_2O_2 (20 µM), Ampliflu™ Red (20 µM) and HRP (0.02 U/mL) and a single compound of interest (50 µM or 5 µM, 1% DMSO (v/v)). The control wells contained same amount of DMSO (1% (v/v)) without any inhibitor. Fluorometric determination of the remaining HRP activity was followed by the fluorescence of the resorufin formed (excitation at 535 nm, emission at 595 nm) at 30°C.

5.2.2. Monoamine oxidase activity assay

The spectrophotometric assays for purified human MAO-A and for membrane-bound human MAO-A/MAO-B are based on the conversion of kynuramine to 4-hydroxyquinoline using reported conditions.[51,60] The spectrophotometric assay for purified human MAO-A activity in a final volume of 200 µL 50 mM potassium phosphate buffer (pH 7.4) contained kynuramine (0.3 mM, equivalent to $2\times K_M$) as the substrate and purified MAO-A (52 nM). The absorbance change at 30°C was followed at 314 nm in the Uvikon 2101 spectrophotometer

The spectrophotometric assay for membrane-bound human MAO-A and MAO-B was measured at 314 nm and 30°C in a Uvikon 2101 spectrophotometer. In a final volume of 0.4 mL 50 mM potassium phosphate pH 7.5, kynuramine was fixed at $2\times K_M$ and inhibitor concentration varied over 4 orders of magnitude. Membrane-bound MAO-A was used at 1/4000 and MAO-B at 1/2000 of the supplied suspension. The final kynuramine concentrations were 60 µM for MAO-A and 30 µM for MAO-B. The linear rates from 8-10 assays were plotted against the log of inhibitor concentration and analysed using non-linear regression (3-parameter equation) in GraphPad Prism 4 software with the bottom fixed at zero. The IC_{50} values are shown with the standard error of the parameter estimate.

5.2.3. ABAD activity assay

A modified version of ABAD activity assay has been used to determine inhibitory effect of discussed compounds.[26] In-house assay reaction conditions consisted of ABAD enzyme (0.5 μg/mL), NADH (250 μM), acetoacetyl-CoA (120 μM) and a single compound of interest (100 μM, 1% DMSO (v/v)). Solutions were prepared in assay buffer (10 mM HEPES buffer, 0.5% (w/v) gelatin (porcine skin), pH 7.4 at 37°C). Control solutions containing an equivalent concentration of DMSO (1% (v/v)) were also prepared and run concurrently. Reaction progression was measured via a decrease in NADH absorbance at 340 nm using a SpectraMAX M2e spectrophotometer. The reaction period was gated to yield steady state conditions (R^2 > 0.9). Assay validity was demonstrated on compound AG18051[43] and experimental data were included in Supplementary Information (Fig. S1).

5.3. Cell viability assessment

Standard MTT assay (Sigma Aldrich) was used according to the manufacturer's protocol on the CHO-K1 cell line (Chinese hamster ovary, ECACC, Salisbury, UK) in order to compare the cytotoxic effect of studied compounds. The cells were cultured according to ECACC recommended conditions and seeded in a density of 8000 per well as was described earlier.[52] Briefly, tested compounds were dissolved in DMSO and subsequently in the growth medium (F-12) supplemented with 10% FBS and 1% PEN/STREP so that the final concentration of DMSO did not exceed 0.5% (v/v). Cells were exposed to the tested compounds in the medium (100 μL) for 24 hours. Then this medium was replaced by the medium containing 10 μM of MTT (100 μL) and cells were allowed to produce formazan for another approximately 3 h under surveillance. Thereafter, medium with MTT was removed and crystals of formazan were dissolved in DMSO (100 μL). Cell viability was assessed spectrophotometrically by the amount of formazan produced. Absorbance was measured at 570 nm, with 650 nm as a reference wavelength on Synergy HT reader (BioTek, USA). LC_{50} was then calculated from the control - subtracted triplicates using non-linear regression (four parameters) of GraphPad Prism 5 software. Final LC_{50} and SEM value was obtained as a mean of 3 independent measurements. MTT assay was validated with simultaneous tacrine LC_{50} determination, which is in agreement with those reported in literature.[49] Triton X (0.1%) has been used as negative control for MTT assay, confirming 100% of cells death.

5.4. Prediction of blood-brain barrier permeation

5.4.1. Chemicals and instrumentation

In LC-UV-MS analyses, acetonitrile, formic acid, both of LC-MS grade purity (Sigma Aldrich), and ultrapure water of ASTM I type (resistance 18.2 MΩ.cm at 25°C) prepared by Barnstead Smart2Pure 3 UV/UF (ThermoFisher Scientific, Bremen, Germany) apparatus were used for preparation of mobile phases.

5.4.2. Parallel artificial membrane permeation assay

A modification of the parallel artificial membrane permeation assay (PAMPA) has been used based on reported protocol.[54] The filter membrane of the donor plate was coated with PBL (Polar Brain Lipid, Avanti, USA) in dodecane (4 µL of 20 mg/mL PBL in dodecane) and the acceptor well was filled with 300 µL of PBS pH 7.4 buffer (V_D). Tested compound were dissolved first in DMSO and then diluted with PBS pH 7.4 to reach the final concentration 25 µM in the donor well. Concentration of DMSO did not exceed 0.5% (V/V) in the donor solution. 300 µL of the donor solution was added to the donor wells (V_A) and the donor filter plate was carefully put on the acceptor plate so that the coated membrane was "in touch" with both donor solution and acceptor buffer. Test compound diffused from the donor well through the lipid membrane (Area = 0.28 cm^2) to the acceptor well. The concentration of the drug in both donor and the acceptor wells was assessed after 3, 4, 5 and 6 hours of incubation in quadruplicate using HPLC. Concentration of the compounds was calculated from the standard curve and expressed as the permeability (P_e) according the following equation.[55,56]

$$\log P_e = \log \left\{ C \times -ln\left(1 - \frac{[drug]_{acceptor}}{[drug]_{equilibrium}}\right)\right\} where\ C = \left(\frac{V_D \times V_A}{(V_D + V_A) \times area \times time}\right)$$

5.4.3. HPLC analysis

HPLC analysis of the donor and acceptor solutions from the PAMPA assay was carried out using a Dionex UltiMate 3000 analytical system equipped with a Waters Atlantis dC18 (2.1 x 100 mm/3 µm) column as the stationary phase. The elution was performed by a linear gradient method utilizing ultra-pure water (MPA) and acetonitrile (MPB), both acidified with 0.1% (v) of formic acid. For the elution, following simple program was developed: 0-1.0 min 10% MPB, 1.0-4.0 min 10-100% MPB, 4.0-5.0 min 100% MPB, 5.0-5.0 min 10% MPB, 5.0-7.5 min 10% MPB.[52] This 7.5 min long analytical method with mobile phase flow-rate set to 0.4 mL/min and injection volume to 5 µL enabled to achieve relatively high sensitivity in UV-detection at the wavelength of 278 nm, which was desirable especially for quantification of the analytes in the acceptor well. In order to determine the unknown concentrations of the studied compounds in the donor and acceptor solutions, an 8-level calibration measurement spanning range of 0.1 – 50 µg/mL was carried out. The linearity of calibration for all compounds was confirmed with R^2 > 0.999. Processing of UV-chromatograms and quantification was carried out in Chromeleon 6.80. This HPLC method was also employed for uncalibrated purity evaluation (at the wavelength of 254 nm) and for HRMS determination of the studied compounds by coupling the analytical system with a Q Exactive Plus mass spectrometer. The obtained mass spectra were processed in Xcalibur 3.0.63 software.

5.5. Molecular docking

Structure models of MAO-A (PDB ID: 2Z5X, resolution: 2.2 Å) and MAO-B (PDB ID: 2V5Z, resolution: 1.6 Å) have been obtained from online PDB database (www.rcsb.org). The protein structure preparation process included removal of ligands, residual waters and additive co-crystallized molecules, merging of non-polar hydrogens, addition of polar hydrogens and assignment of default Gastaiger charges. Further protein structure processing for flexible molecular docking was performed with MGL Tools Receptor Python scripts. A cavity in 2Z5X was approximated by a docking grid box with 35 Å long edge centered at N5 FAD atom (x = 34.176, y = 31.342, z = -14.785). Analogically, a grid box of the same size was centred at x = 52.895, y = 158.664, z = 27.672 within MAO-B 3D model. The ligand **19** was drawn in HyperChem 8.0 and geometrically optimized with PM3 semi-empirical method employing Polak-Ribiere conjugate gradient algorithm. The structure of ligand was further processed utilizing MGL Tools Ligand Python scripts. Molecular docking runs were performed in AutoDock Vina (v1.1.2) using 24 CPUs in parallel with the exhaustiveness parameter set to 128.[61] Several of the cavity forming residues (MAO-A: Tyr69, Leu97, Gln99, Val101, Phe173, Ile180, Asn181, Ile207, Phe208, Ser209, Val210, Gln215, Lys305, Cys323, Met324, Ile325, Glu327, Ile335, Thr336, Leu337, Met350, Phe352, Tyr407, Tyr444; MAO-B: Ser59, Tyr60, Gln65, His90, Phe99, Phe103, Trp119, Leu164, Leu167, Phe168, Leu171, Cys172, Ile198, Ile199, Ser200, Gln206, Lys296, Ile316, Tyr326, Phe343, Tyr398, Tyr435) were assigned as flexible ones. Flexible docking was repeated 10 times for both enzymes and the top-scored poses were visually inspected with figures generation using PyMOL (v1.7). In each docking run, 9 binding modes with the lowest binding energies were stored to evaluate all significantly contributing ligand-enzyme interactions.

References

1. Goedert, M.; Spillantini, M. G. *Science (80-.).* **2006**, *314*, 777–781.
2. De-Paula, V.; Radanovic, M.; Diniz, B. S.; Forlenza, O. V In *Protein Aggregation and Fibrillogenesis in Cerebral and Systemic Amyloid Disease*; Harris, J. R., Ed.; Springer Netherlands, **2012**; Vol. 65, pp. 329–352.
3. Blennow, K.; de Leon, M. J.; Zetterberg, H. *Lancet* **2006**, *368*, 387–403.
4. Barage, S. H.; Sonawane, K. D. *Neuropeptides* **2015**, *52*, 1–18.
5. van Marum, R. J. *Fundam. Clin. Pharmacol.* **2008**, *22*, 265–274.
6. Munoz-Torrero, D. *Curr. Med. Chem.* **2008**, *15*, 2433–2455.
7. Dringenberg, H. C. *Behav. Brain Res.* **2000**, *115*, 235–249.
8. Youdim, M. B. H.; Edmondson, D.; Tipton, K. F. *Nat. Rev. Neurosci.* **2006**, *7*, 295–309.
9. Shih, J. C.; Chen, K.; Ridd, M. J. *Annu. Rev. Neurosci.* **1999**, *22*, 197–217.
10. Ramsay, R. R. Monoamine Oxidases: The Biochemistry of the Proteins As Targets in Medicinal Chemistry and Drug Discovery. *Curr. Top. Med. Chem.* **2012**, *12*, 2189–2209.
11. Sparks, D. L.; Woeltz, V. M.; Markesbery, W. R. *Arch. Neurol.* **1991**, *48*, 718–721.

12. Jossan, S. S.; Gillberg, P. G.; Gottfries, C. G.; Karlsson, I.; Oreland, L. *Neuroscience* **1991**, *45*, 1–12.

13. Emilsson, L.; Saetre, P.; Balciuniene, J.; Castensson, A.; Cairns, N.; Jazin, E. E. *Increased monoamine oxidase messenger RNA expression levels in frontal cortex of Alzheimer's disease patients*; **2002**; Vol. 326.

14. Kennedy, B. P.; Ziegler, M. G.; Alford, M.; Hansen, L. A.; Thal, L. J.; Masliah, E. *J. Neural Transm.* **2003**, *110*, 789–801.

15. Burke, W. J.; Li, S. W.; Schmitt, C. A.; Xia, P.; Chung, H. D.; Gillespie, K. N. *Brain Res.* **1999**, *816*, 633–637.

16. Yan, M. H.; Wang, X.; Zhu, X. *Free Radic. Biol. Med.* **2013**, *62*, 90–101.

17. Hardy, J. A.; Higgins, G. A. *Science (80-.).* **1992**, *256*, 184–185.

18. Bayer, T. A.; Wirths, O. *Front. Aging Neurosci.* **2010**, *2*, 10.

19. Du, H.; Guo, L.; Yan, S. Q.; Sosunov, A. A.; McKhann, G. M.; Yan, S. S. *Proc. Natl. Acad. Sci. U. S. A.* **2010**, *107*, 18670–18675.

20. Manczak, M.; Anekonda, T. S.; Henson, E.; Park, B. S.; Quinn, J.; Reddy, P. H. *Hum. Mol. Genet.* **2006**, *15*, 1437–1449.

21. Du, H.; Guo, L.; Yan, S. S. *Antioxid. Redox Signal.* **2012**, *16*, 1467–1475.

22. Benek, O.; Aitken, L.; Hroch, L.; Kuca, K.; Gunn-Moore, F.; Musilek, K. *Curr. Med. Chem.* **2015**, *22*, 1056–1085.

23. Yan, S. D.; Fu, J.; Soto, C.; Chen, X.; Zhu, H. J.; AlMohanna, F.; Collison, K.; Zhu, A. P.; Stern, E.; Saido, T.; Tohyama, M.; Ogawa, S.; Roher, A.; Stern, D.; Du Yan, S.; Fu, J.; Soto, C.; Chen, X.; Zhu, H. J.; Al-Mohanna, F.; Collison, K.; Zhu, A. P.; Stern, E.; Saido, T.; Tohyama, M.; Ogawa, S.; Roher, A.; Stern, D. *Nature* **1997**, *389*, 689–695.

24. Lustbader, J. W.; Cirilli, M.; Lin, C.; Xu, H. W.; Takuma, K.; Wang, N.; Caspersen, C.; Chen, X.; Pollak, S.; Chaney, M.; Trinchese, F.; Liu, S. M.; Gunn-Moore, F.; Lue, L. F.; Walker, D. G.; Kuppusamy, P.; Zewier, Z. L.; Arancio, O.; Stern, D.; Yan, S. S. D.; Wu, H. *Science (80-.).* **2004**, *304*, 448–452.

25. Yao, J.; Du, H.; Yan, S. Q.; Fang, F.; Wang, C. D.; Lue, L. F.; Guo, L.; Chen, D.; Stern, D. M.; Gunn-Moore, F.; Chen, J. X.; Arancio, O.; Yan, S. S. *J. Neurosci.* **2011**, *31*, 2313–2320.

26. Yan, S. D.; Shi, Y. G.; Zhu, A. P.; Fa, J.; Zhu, H. J.; Zhu, Y. C.; Gibson, L.; Stern, E.; Collison, K.; Al-Mohanna, F.; Ogawa, S.; Roher, A.; Clarke, S. G.; Stern, D. M. *J. Biol. Chem.* **1999**, *274*, 2145–2156.

27. Takuma, K.; Yao, J.; Huang, J. M.; Xu, H. W.; Chen, X.; Luddy, J.; Trillat, A. C.; Stern, D. M.; Arancio, O.; Yan, S. S. D. *FASEB J.* **2005**, *19*, 597–598.

28. Lim, Y. A.; Grimm, A.; Giese, M.; Mensah-Nyagan, A. G.; Villafranca, J. E.; Ittner, L. M.; Eckert, A.; Gotz, J. *PLoS One* **2011**, *6*, 12.

29. Marques, A. T.; Fernandes, P. A.; Ramos, M. J. *Mini-Reviews Med. Chem.* **2009**, *9*, 1002–1008.

30. Youdim, M. B. H.; Buccafusco, J. J. *Trends Pharmacol. Sci.* **2005**, *26*, 27–35.

31. Cavalli, A.; Bolognesi, M. L.; Minarini, A.; Rosini, M.; Tumiatti, V.; Recanatini, M.; Melchiorre, C. *J. Med. Chem.* **2008**, *51*, 347–372.

32. Luo, W.; Li, Y. P.; He, Y.; Huang, S. L.; Tan, J. H.; Ou, T. M.; Li, D.; Gu, L. Q.; Huang, Z. S. *Bioorg. Med. Chem.* **2011**, *19*, 763–770.

33. Fang, L.; Appenroth, D.; Decker, M.; Kiehmopf, M.; Roegler, C.; Deufel, T.; Fleck, C.; Peng, S. X.; Zhang, Y.; Lehmann, J. *J. Med. Chem.* **2008**, *51*, 713–716.

34. Marco-Contelles, J.; Leon, R.; de los Rios, C.; Guglietta, A.; Terencio, J.; Lopez, M. G.; Garcia, A. G.;

Villarroya, M. *J. Med. Chem.* **2006**, *49*, 7607–7610.

35. Bolea, I.; Juarez-Jimenez, J.; de los Rios, C.; Chioua, M.; Pouplana, R.; Luque, F. J.; Unzeta, M.; Marco-Contelles, J.; Samadi, A. *J. Med. Chem.* **2011**, *54*, 8251–8270.

36. Sterling, J.; Herzig, Y.; Goren, T.; Finkelstein, N.; Lerner, D.; Goldenberg, W.; Miskolczi, I.; Molnar, S.; Rantal, F.; Tamas, T.; Toth, G.; Zagyva, A.; Zekany, A.; Lavian, G.; Gross, A.; Friedman, R.; Razin, M.; Huang, W.; Krais, B.; Chorev, M.; Youdim, M. B.; Weinstock, M. *J. Med. Chem.* **2002**, *45*, 5260–5279.

37. Youdim, M. H.; Amit, T.; Bar-Am, O.; Weinreb, O.; Yogev-Falach, M. *Neurotox. Res.* **2006**, *10*, 181–192.

38. Xie, Y. L.; Deng, S. M.; Chen, Z. Z.; Yan, S. D.; Landry, D. W. *Bioorg. Med. Chem. Lett.* **2006**, *16*, 4657–4660.

39. Valasani, K. R.; Hu, G.; Chaney, M. O.; Yan, S. S. *Chem. Biol. Drug Des.* **2013**, *81*, 238–249.

40. Valasani, K. R.; Sun, Q.; Hu, G.; Li, J.; Du, F.; Guo, Y.; Carlson, E. A.; Gan, X.; Yan, S. S. *Curr. Alzheimer Res.* **2014**, *11*, 9.

41. Hroch, L.; Benek, O.; Guest, P.; Aitken, L.; Soukup, O.; Janockova, J.; Musil, K.; Dohnal, V.; Dolezal, R.; Kuca, K.; Smith, T. K.; Gunn-Moore, F.; Musilek, K. *Bioorg. Med. Chem. Lett.* **2016**, *26*, 3675–3678.

42. Perez, V.; Marco, J. L.; Fernandez-Alvarez, E.; Unzeta, M. *Br. J. Pharmacol.* **1999**, *127*, 869–876.

43. Kissinger, C. R.; Rejto, P. A.; Pelletier, L. A.; Thomson, J. A.; Showalter, R. E.; Abreo, M. A.; Agree, C. S.; Margosiak, S.; Meng, J. J.; Vanderpool, R.; Li, B.; Tempczyk-Russell, A.; Villafranca, J. E. *J. Mol. Biol.* **2004**, *342*, 943–952.

44. Munch, H.; Hansen, J. S.; Pittelkow, M.; Christensen, J. B.; Boas, U. *Tetrahedron Lett.* **2008**, *49*, 3117–3119.

45. Wong, R.; Dolman, S. J. *J. Org. Chem.* **2007**, *72*, 3969–3971.

46. Busacca, C. A.; Milligan, J. A.; Rattanangkool, E.; Ramavarapu, C.; Chen, A.; Saha, A. K.; Li, Z.; Lee, H.; Geib, S. J.; Wang, G.; Senanayake, C. H.; Wipf, P. *J. Org. Chem.* **2014**, *79*, 9878–87.

47. Zhou, M.; Diwu, Z.; Panchuk-Voloshina, N.; Haugland, R. P. *Anal. Biochem.* **1997**, *253*, 162–8.

48. Holt, A.; Palcic, M. M. *Nat. Protoc.* **2006**, *1*, 2498–2505.

49. Benek, O.; Soukup, O.; Pasdiorova, M.; Hroch, L.; Sepsova, V.; Jost, P.; Hrabinova, M.; Jun, D.; Kuca, K.; Zala, D.; Ramsay, R. R.; Marco-Contelles, J.; Musilek, K. *ChemMedChem* **2016**, *11*, 1264–1269.

50. Kabeya, L. M.; de Marchi, A. A.; Kanashiro, A.; Lopes, N. P.; da Silva, C.; Pupo, M. T.; Lucisano-Valima, Y. M. *Bioorg. Med. Chem.* **2007**, *15*, 1516–1524.

51. Tan, A. K.; Ramsay, R. R. *Biochemistry* **1993**, *32*, 2137–2143.

52. Malinak, D.; Dolezal, R.; Marek, J.; Salajkova, S.; Soukup, O.; Vejsova, M.; Korabecny, J.; Honegr, J.; Penhaker, M.; Musilek, K.; Kuca, K. *Bioorg. Med. Chem. Lett.* **2014**, *24*, 5238–5241.

53. Lühr, S.; Vilches-Herrera, M.; Fierro, A.; Ramsay, R. R.; Edmondson, D. E.; Reyes-Parada, M.; Cassels, B. K.; Iturriaga-Vásquez, P. *Bioorg. Med. Chem.* **2010**, *18*, 1388–1395.

54. Di, L.; Kerns, E. H.; Fan, K.; McConnell, O. J.; Carter, G. T. *Eur. J. Med. Chem.* **2003**, *38*, 223–232.

55. Sugano, K.; Hamada, H.; Machida, M.; Ushio, H. *J. Biomol. Screen.* **2001**, *6*, 189–196.

56. Wohnsland, F.; Faller, B. *J. Med. Chem.* **2001**, *44*, 923–930.

57. Jones, T. Z. E.; Fleming, P.; Eyermann, C. J.; Gravestock, M. B.; Ramsay, R. R. *Biochem. Pharmacol.* **2005**, *70*, 407–416.

58. Juárez-Jiménez, J.; Mendes, E.; Galdeano, C.; Martins, C.; Silva, D. B.; Marco-Contelles, J.; do Carmo

Carreiras, M.; Luque, F. J.; Ramsay, R. R. *Biochim. Biophys. Acta - Proteins Proteomics* **2014**, *1844*, 389–397.

59. Violante-Mota, F.; Tellechea, E.; Moran, J. F.; Sarath, G.; Arredondo-Peter, R. *Phytochemistry* **2010**, *71*, 21–6.

60. Weissbach, H.; Smith, T. E.; Daly, J. W.; Witkop, B.; Udenfriend, S. *J. Biol. Chem.* **1960**, *235*, 1160–1163.

61. Trott, O.; Olson, A. J. *J. Comput. Chem.* **2010**, *31*, 455–461.

Graphical abstract

Synthesis and evaluation of frentizole-based indolyl thiourea analogues as MAO/ABAD inhibitors for Alzheimer's disease treatment

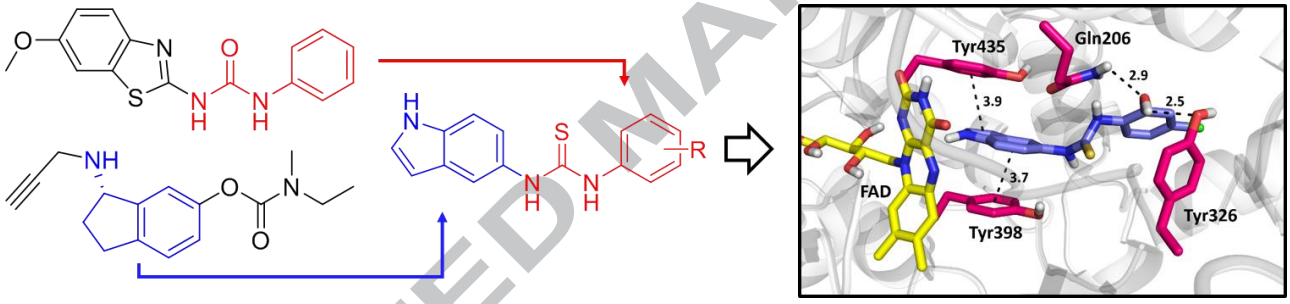

Highlights

- Novel frentizole-based indolyl thiourea analogues were prepared as potential MAO/ABAD inhibitors.
- Compound **19** displayed low micromolar and high nanomolar IC_{50} value for MAO-A and MAO-B inhibition.
- Compounds **17** and **21** showed important structural features for future design of ABAD inhibitors.
- Several reported compounds acted as low micromolar HRP inhibitors.
- The active compounds demonstrated low cytotoxicity profile.